Changes in Submicrometer Structure of Enzymatically Hydrolyzed Microcrystalline Cellulose

ARTICLE *in* BIOMACROMOLECULES · MARCH 2010

Impact Factor: 5.75 · DOI: 10.1021/bm1001119 · Source: PubMed

Changes in Submicrometer Structure of Enzymatically Hydrolyzed Microcrystalline Cellulose

Paavo A. Penttilä,*[,†,‡] Anikó Várnai,[§] Kirsi Leppänen,[†] Marko Peura,[†] Aki Kallonen,[†] Pentti Jääskeläinen,[||] Jessica Lucenius,[†] Janne Ruokolainen,[⊥] Matti Siika-aho,[#] Liisa Viikari,[§] and Ritva Serimaa[†]

Departments of Physics and Food and Environmental Sciences, University of Helsinki, Helsinki, Finland, Departments of Biomedical Engineering and Computational Science and Applied Physics, Aalto University School of Science and Technology, Espoo, Finland, and VTT Technical Research Centre of Finland, Espoo, Finland

Received January 29, 2010; Revised Manuscript Received March 5, 2010

To understand the limitations occurring during enzymatic hydrolysis of cellulosic materials in renewable energy production, we used wide-angle X-ray scattering (WAXS), small-angle X-ray scattering (SAXS), X-ray microtomography, and transmission electron microscopy (TEM) to characterize submicrometer changes in the structure of microcrystalline cellulose (Avicel) digested with the *Trichoderma reesei* enzyme system. The microtomography measurements showed a clear decrease in particle size in scale of tens of micrometers. In all the TEM pictures, similar elongated and partly ramified structures were observed, independent of the hydrolysis time. The SAXS results of rewetted samples suggested a slight change in the structure in scale of 10−20 nm, whereas the WAXS results confirmed that the degree of crystallinity and the crystal sizes remained unchanged. This indicates that the enzymes act on the surface of cellulose bundles and are unable to penetrate into the nanopores of wet cellulose.

Introduction

Cellulose, the most abundant biopolymer on earth, can be used as a renewable energy source. Cellulosic materials can be hydrolyzed into fermentable sugars, which can be further utilized as raw material for biofuel production. In second gereneration biorefineries one of the aims is to use agricultural or forest industry waste materials not competing with food production. Until today, most of the raw materials for production of biofuels originate from food plants, which cannot be considered a sustainable solution.[1,2]

The hydrolysis of cellulose can be carried out with the aid of acids or cellulase enzymes. Though the processes have been investigated already for several decades, unanswered questions still remain, concerning especially the reaction rates and the physicochemical interactions between the enzymes and the substrate material.[3] It has been discovered that the reactions are strongly affected by the physicochemical properties and the morphology of the substrate.[4] These parameters influence the accessibility of the enzymes to the substrate and they may also change during the reaction. The changes in cellulase activity and availability might be responsible for the gradual slowing down of the reaction, which is presently one of the main factors retarding the full use of the method. The accessibility of cellulose is also an important factor related to this subject, because the hydrolysis is a two-phase reaction.[5,6]

Several properties such as crystallinity, degree of polymerization, surface area, porosity, and particle size and their effects on the rates of hydrolysis have been investigated.[2,4,5,7] For instance, in the case of a partly crystalline substrate, such as microcrystalline cellulose (MCC), a higher degree of crystallinity seems to reduce the surface area suitable for binding of the enzymes and in this way hinders the reaction.[5] However, this is not necessarily true for all cellulosic substrates.[6] Concerning the possible change in the degree of crystallinity or the dimensions of the crystallites during hydrolysis, diverse results for different substrates have been obtained. Some studies have shown that the crystallinity has slightly increased,[7,8] while others have reported that it has remained unchanged during the hydrolysis.[4] Likewise, the average crystal size determined from the 200 reflection, that is, the width of the crystallites, has decreased,[4,7] remained unchanged,[4] or even increased with the hydrolysis.[8] A logical explanation for most of the changes would be the more readily hydrolyzable amorphous parts in cellulose microfibrils, which would be hydrolyzed faster, leaving proportionally more crystalline cellulose behind.[8] However, this hypothesis has been questioned, because some findings indicate that the crystallinity of cellulose does not change appreciably during enzymatic hydrolysis.[9]

In a larger scale, the morphology of the cellulose particles becomes an important factor. Because the average diameter of cellulolytic enzymes is as high as 5.9 nm,[10] the accessibility of the enzymes to the substrate is highly dependent on the roughness of the surface and on the pore structure of the substrate particles. According to previous studies, in which the crystallinities remained the same and the surface roughness increased, the hydrolysis of microcrystalline cellulose is supposed to take place in the outer layer of the particle surface

* To whom correspondence should be addressed. E-mail: paavo.a.penttila@helsinki.fi.
[†] Department of Physics, University of Helsinki.
[‡] POB 64, FI-00014 University of Helsinki, Finland.
[§] Department of Food and Environmental Sciences, University of Helsinki.
[||] Department of Biomedical Engineering and Computational Science, Aalto University School of Science and Technology.
[⊥] Department of Applied Physics, Aalto University School of Science and Technology.
[#] VTT Technical Research Centre of Finland.

10.1021/bm1001119
Published on Web 03/23/2010

and to proceed layer by layer.[7] Furthermore, the smaller and more readily accessible particles would be hydrolyzed faster, which causes that the average parameters remain as there is always a larger proportion of completely intact particles in the sample.[4]

In this study, the effects of enzymatic hydrolysis on the structure of microcrystalline cellulose were investigated with a purpose to find new insights into the limiting factors, especially related to the substrate structure, responsible for the gradual slowing down of the process. The used enzymes originated from the *Trichoderma reesei* species and the hydrolysis times varied between 6 and 75 h, eventually leading to a 68% degree of hydrolysis. The main characterization was done with X-ray scattering methods, wide- and small-angle X-ray scattering (WAXS and SAXS). They have been widely used for similar purposes and they have proved to be suitable for studies of partly crystalline and highly hierarchical biological soft matter.[4,7,11,12] In addition to the scattering methods, the morphology of the samples was studied with X-ray microtomography and transmission electron microscopy (TEM).

Experimental Section

Enzymatic Hydrolysis. The starting material of the hydrolysis was commercially available microcrystalline cellulose, Avicel (14204, SERVA Electrophoresis), with a particle size of 0.05 mm. Avicel was hydrolyzed with a mixture of commercial enzyme preparations (Celluclast 1.5 L and Novozym 188 by Novozymes, Denmark) at a loading of Celluclast (10 FPU/g dry weight substrate) supplemented with Novozym 188 β-glucosidase (100 nkat/g dry weight), corresponding to a total load of 20 mg protein/g of glucan. The cellulases originated from the *Trichoderma reesei* enzyme system and the β-glucosidase from *Aspergillus niger*. The hydrolyses were carried out in 50 mM sodium-citrate buffer, pH adjusted to 5.0, shaken at 130 rpm at 45 °C, with 1% substrate consistency. After hydrolysis, the samples were boiled for 10 min to inactivate the enzymes, then filtered through a 60 μm filter. The hydrolysis residue was freeze-dried for the X-ray and TEM measurements.

The enzymatic hydrolyses for samples after 6, 24, and 75 h of hydrolysis were evaluated on the basis of reducing sugars liberated, using the DNS method.[13] The degree of hydrolysis was calculated as the percentage solubilized of the total dry weight. The hydrolysis was originally done in duplicates, but the parallel hydrolysis residues were mixed before freeze-drying.

WAXS Measurements. For the WAXS measurements, the samples were prepared by pressing the sample powders by hand into metal rings of a thickness of 1.5 mm and covering them on both sides with Mylar foil. The radiation was produced by an X-ray generator (UltraX18S, Rigaku) with a rotating copper anode. The beam was monochromated with a Si(111) crystal and a totally reflecting mirror, thus, singling out the Cu Kα radiation (λ = 1.541 Å). After the sample, the scattered radiation was detected with an image plate detector (MAR345, Marresearch) in perpendicular transmission geometry. Each sample was measured for 30 min in room temperature. In addition, the air scattering with Mylar foils and the "dark current" produced mainly by the image reading process of the detector were measured and taken into account in the analysis of the results. The instrumental broadening of the measurement device, which was determined to be approximately 0.3° at the scattering angle $2\theta = 28°$ by measuring a silicon sample, was also considered during the analysis.

The 004 reflection ($2\theta = 35°$) was measured separately with a four-circle diffractometer, which included a four-circle goniometer (420/511, Huber), an X-ray generator (Siemens), a sealed X-ray tube with a copper anode, a ground, and bent germanium monochromator, and a NaI(Tl) scintillation counter. For these measurements, the sample powders were pressed as thin plates in metal holders and they were measured in symmetrical transmission geometry. The instrumental broadening was determined by measuring a sample of hexamethyltetramine ($C_6H_{12}N_4$).

SAXS Measurements. The SAXS measurements were carried out on the same samples as the WAXS measurements. In addition, the measurements were repeated with rewetted samples. These were prepared by immersing the once freeze-dried powders for a week in water with a concentration of approximately 3 wt %. The excess water was removed right before the measurements and the swollen powders were placed in metal rings and sealed with Mylar foil, similarly to the dry samples.

The SAXS measurement apparatus consisted of an X-ray generator (Siemens) with an X-ray tube with a copper anode (Panalytical) and a two-dimensional wire detector (HI-STAR, Bruker AXS). The operational voltage and current of the generator were 36 kV and 25 mA, respectively. The monochromated beam was point-collimated and the measurement geometry was a perpendicular transmission. Besides the three dry and three wet samples, the scattering of an empty metal ring covered with Mylar foil was measured for the background correction. The measurement time was 60 min for each. The measured q-values were in the range of 0.014−0.22 1/Å, with the definition $q = (4\pi \sin \theta)/(\lambda)$ for the length of the scattering vector. A piece of Lupolen was used as a standard in scaling the intensities to absolute scale.[12] The measurement program made spatial and flood-field corrections for the data.

Microtomography Measurements. The measurement system was a custom-made X-ray microtomography device (nanotom180 NF, Phoenix|X-ray Systems + Services), including a flat panel CMOS detector (Hamamatsu) with 2304 × 2304 pixels (pixel size 50 μm). The X-ray tube had a tungsten anode and its operational voltage and current were 60 kV and 400 μA, respectively. The X-ray beam was approximately conical in shape, making it possible to image samples in μm-resolution by utilizing geometric magnification (see, e.g., Stock[14]). Here this magnification was 50.

The sample powders were encapsulated into Eppendorf tubes which were attached to the sample holder of the tomography device using beeswax. In the measurements, 1440 absorption images (projections) were acquired in 0.25 degree steps over a full circle of rotation. Each projection was an average of five individual images of 750 ms exposure time. Three-dimensional reconstructions were made with the program datos|x (version 1.3.2.11) supplied by Phoenix|X-ray Systems + Services. The voxel size of the reconstructions was the same as the pixel size of the projections, 1.00 μm. The reconstructed volumes were visualized using the program VGStudio MAX 1.2.1 (Volume Graphics GmbH, Germany).

Cryo-TEM Measurements. The sample powders were immersed in water for about one week before the measurements. Thereafter, 3 mL of sample solution was applied on the holey carbon EM grids and vitrified using a FEI Vitrobot: excess water was removed by blotting the grids several times for a duration of 1 s, after which the grids were plunged in a mixture of liquid ethane and propane at temperature of −180 °C. The grids with vitrified sample solution were maintained at liquid nitrogen temperature and then cryo transferred into the microscope using Gatan 910 cryo-transfer holder at temperature of about −185 °C. The samples were imaged with a FEI Tecnai 12 bright-field transmission electron microscope with a LaB_6 filament. The electrons were accelerated with a voltage of 120 kV and they were detected after the sample with a CCD camera (Ultrascan 1000, Gatan) with a pixel size of 14 μm and a 16 bit dynamic range. The image magnifications varied from less than 1000× to 62000×.

Data Analysis. *WAXS Analysis.* The integrated intensities were corrected for absorption, measuring geometry, and scattering by air and Mylar foils. When determining the crystal sizes, an amorphous background intensity was subtracted from the data. The background was the measured scattering of a sulfate lignin sample, which has proved to be a suitable approximation for the amorphous background of MCC samples.[15]

Table 1. Crystal Size and Degree of Crystallinity of Enzymatically Hydrolyzed MCC Determined by the WAXS Analysis

		crystal size (nm) corresponding to reflections				
hydrolysis time (h)	degree of hydrolysis	$1\bar{1}0$	110	200	004	degree of crystallinity (%)
0[a]		5.0 ± 0.3	5.0 ± 0.4	5.34 ± 0.10		48 ± 3
6	30.8 ± 0.3	4.7 ± 0.3	5.5 ± 0.4	5.36 ± 0.10	21 ± 2	49 ± 3
24	57.9 ± 0.8	4.8 ± 0.3	5.6 ± 0.4	5.24 ± 0.10	22 ± 2	50 ± 3
75	67.6 ± 0.5	4.8 ± 0.3	5.7 ± 0.4	5.27 ± 0.10	24 ± 2	49 ± 3

[a] The corresponding values for nonhydrolyzed MCC, measured earlier.

The crystal sizes were calculated by fitting Gaussian functions to peaks corresponding to the reflections $1\bar{1}0$, 110, and 200 of cellulose Iβ. From the full width at half-maximum (fwhm) and the position of the maximum of the fit, the crystal size corresponding to each reflection could be calculated using the Scherrer equation (eq 1, see Supporting Information for equations and more details on the analysis of scattering data).

The degree of crystallinity was determined by a curve fitting procedure, in which altogether 24 Gaussian functions were fitted to the data corresponding to the theoretical reflections of cellulose.[16] The degree of crystallinity was then calculated as the ratio of the intensity scattered by the crystalline part and the measured intensity, using sulfate lignin again as an approximation for the amorphous part.[15]

The crystal sizes corresponding to the 004 reflection, that is, the average lengths of the crystallites, were determined from the four-circle diffractometer measurements. The amorphous background was assumed to be linear near this reflection and the crystal lengths were calculated using the Scherrer equation (eq 1).

SAXS Analysis. The SAXS intensity of a system of two phases with smooth interfaces obeys the Porod law ($I(q) \propto q^{-4}$). When knowing the invariant $Q = \int_0^\infty I(q)q^2\mathrm{d}q$ and the volume fractions of the phases, the specific surface of the system can be calculated from eq 2 in the Supporting Information. One way to gain the invariant Q is presented in eq 3. This approach requires the intensities to be on absolute scale, which can be reached by measuring a reference sample (see eq 4). The specific surfaces for each sample, that is, the surface area in a mass unit of the solid material, presented later in this article, were calculated with eq 5.[12,17,18]

With the Porod law it is also possible to determine the Porod lengths, that is, average chord lengths of the system. These measures tell about the average distances averaged in all directions between interfaces in the system. The average chord lengths for the whole system and separately for both phases were calculated with eqs 6 and 7.[17,19,20]

If the data obeys a power law $I(q) \propto q^{-\alpha}$ with some other power than $\alpha = 4$, the system may contain fractal structures. Such power laws can be visible in any q-region, for which holds $qR_g \gg 1$. Here R_g can be the radius of gyration of the particles in the sample or some other length typical for the dimensions of the phases. The fractal structures can be either mass or surface fractals, which appear as powers $\alpha \leq 3$ and $3 < \alpha < 4$, respectively. The fractal dimensions D_m and D_s for these structures were calculated with eq 8. Large D_s values correspond to smooth surfaced and internally dense particles, smaller D_s values to internally dense particles with rough surfaces. A smaller D_m represents a more open or ramified structure. The special case of integer power $\alpha = 1$ corresponds to thin cylinders or strings and the power $\alpha = 2$ to thin planes or disks.[17,21]

Results

Degrees of Hydrolysis. The samples studied were hydrolyzed for 6, 24, and 75 h, which corresponded to 30.8, 57.9, and 67.6% of hydrolysis degrees, respectively (Table 1). The behavior of the degree of hydrolysis as a function of hydrolysis time is typical: the rate of hydrolysis is relatively fast in the beginning and gradually decreases with time.[7]

WAXS Results. The WAXS curves are presented as the integrated and corrected intensity of the scattered beam I as a function of the scattering angle 2θ (Figure 1). The shapes of the curves are almost identical and their vertical displacements are most likely due to different sample masses. The calculated average crystal sizes in four directions and the degree of crystallinity are shown in Table 1. The error estimates were mainly determined by slightly varying the fitting parameters and observing their influence on the eventual values.

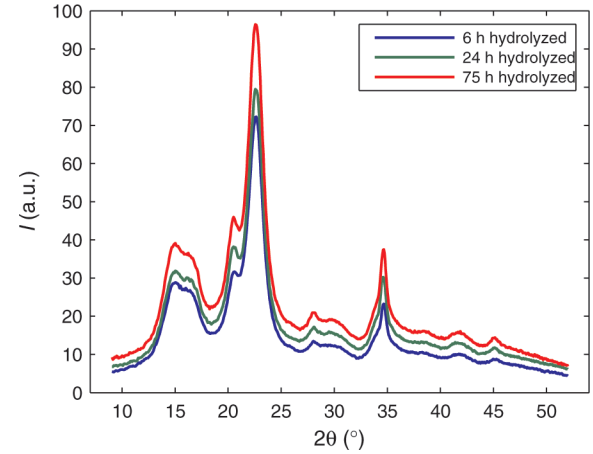

Figure 1. WAXS curves of MCC hydrolyzed enzymatically for various times.

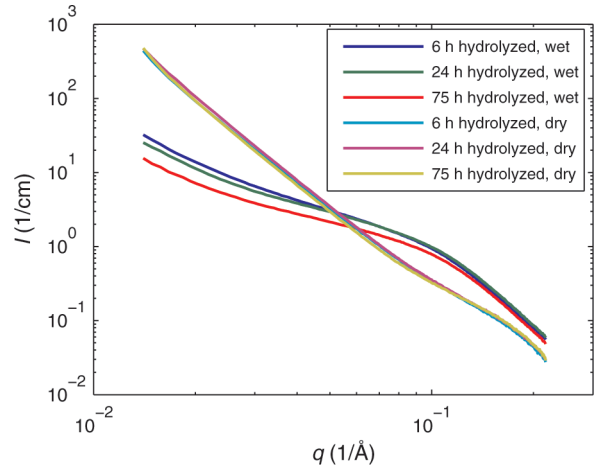

Figure 2. Logarithmic SAXS curves of MCC hydrolyzed enzymatically for various times. A small constant based on Porod's law has been subtracted from the intensities.

SAXS Results. The SAXS curves for both dry and wet samples are presented on a logarithmic scale (Figure 2). The intensities were calculated from the experimental data with eq 4 and they are thus in absolute units (cm^{-1}). The optical thickness of each sample was calculated using values of 3.33 l/cm,[12] 12 l/cm, and 10.4 l/cm[22] for the linear absorption coefficients of Lupolen, cellulose, and water, respectively. The volume fractions were determined with the masses and volumes of the samples, using the density of crystalline cellulose (1.6 g/cm^3) as the density of the solid phase.

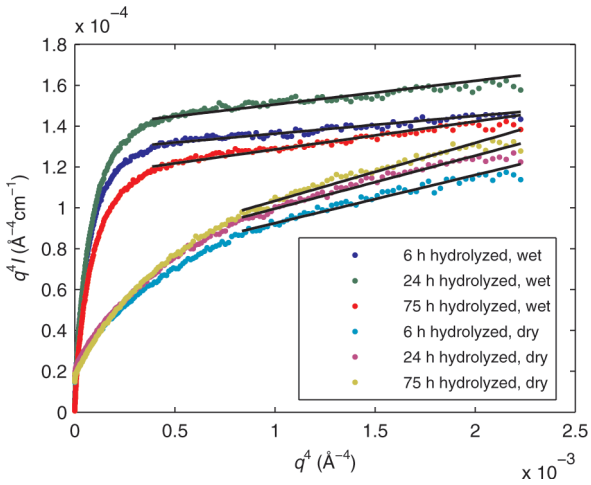

Figure 3. Porod fits for all samples.

Table 2. Powers α Gained from the Power Law Fits on Regions [q_{min}, q_{max}] and the Calculated Fractal Dimensions D

	6 h wet	24 h wet	75 h wet	6 h dry	24 h dry	75 h dry
q_{min} (1/Å)	0.027	0.027	0.027	0.019	0.019	0.019
q_{max} (1/Å)	0.077	0.077	0.077	0.074	0.071	0.071
α	1.5	1.3	1.2	3.5	3.7	3.6
D^a	1.5 (m)	1.3 (m)	1.2 (m)	2.5 (s)	2.3 (s)	2.4 (s)

[a] The letter "m" in brackets stands for mass fractals and the letter "s" stands for surface fractals.

Table 3. Specific Surfaces ($S_{s,m}$) and the Average Chord Lengths for Whole Samples (L_c) and Separately for the Matrix (L_m) and Solid (L_s) Phases

	6 h wet	24 h wet	75 h wet	6 h dry	24 h dry	75 h dry
$S_{s,m}$ (m²/g)	330	410	220	3.3	3.5	3.6
L_c (nm)	6.4	5.2	9.0	140	140	160
L_m (nm)				570	510	430
L_s (nm)				180	200	270

The fitting of Porod's q^{-4} law was carried out for all samples (Figure 3). A constant of order 10^{-2} l/cm was subtracted from the intensity in order to improve the fit.[23] The fitting ranges were $q = 0.140-0.218$ 1/Å for the wet and $q = 0.170-0.218$ 1/Å for the dry samples. These ranges were chosen by following the criteria presented by Vickers et al.[20]

Power laws with other powers than $\alpha = 4$ were fitted to the data on smaller q-values. They were found on slightly different regions for wet and dry samples. These regions as well as the α values and fractal dimensions are presented in Table 2. The fractal dimensions show that the nanoscale structure of the particles in the dry samples is much denser than in the wet samples.

The specific surfaces and average chord lengths calculated from the Porod law fit with eqs 5, 6, and 7 are shown in Table 3. The average chord lengths were calculated from the specific surfaces (eqs 6 and 7) with the aid of the volume fractions of the two phases. Because some inaccuracy was involved in the determination of the volume fractions for the wet samples, the average chord lengths of the phases (L_m and L_s) are not presented in the table. This is also why the results for wet samples in Table 3 should not be compared with each other. On the contrary, the results for dry samples are well comparable between different hydrolysis times, but they may include systematic error of maximum 50% due to the density value of the solid phase used in the calculations. The magnitudes and possible sources of error in the results of Table 3 are further discussed in the Discussion.

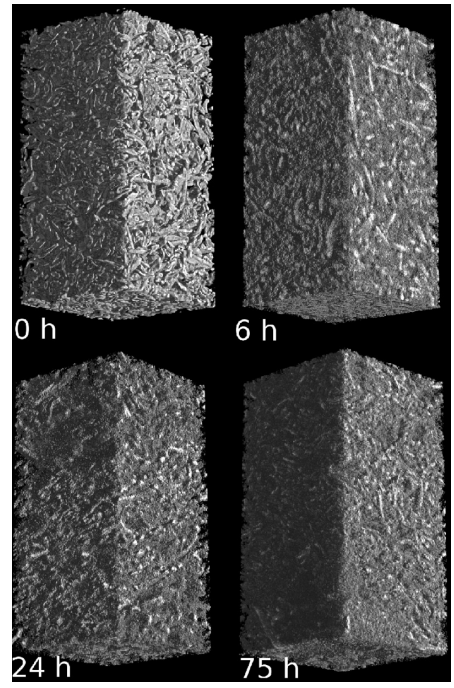

Figure 4. Three-dimensional X-ray microtomography reconstructions from enzymatically hydrolyzed MCC with various hydrolysis times. The native MCC sample was imaged earlier. The dimensions of the reconstructions are 0.5 × 0.5 × 1.0 mm³.

Microtomography and Cryo-TEM Images. The micrometer-size structure of the samples was evaluated using three-dimensional microtomographic reconstructions (Figure 4) as well as cross sections of these reconstructions. The microtomography images are suitable for qualitative comparison between the samples with various hydrolysis degrees. From the images a clear decrease of particle size could be seen in the micrometer scale. Also, the boundaries of the particles were more irregular and fuzzy in the hydrolyzed samples. However, because the voxel size of the reconstruction was 1.00 μm, structures smaller than that could not be distinguished in the images.

The TEM images showed elongated sheet-like structures in various length scales (Figure 5). In pictures with lower magnification, these particles had widths in the order of 1 μm, whereas their lengths were approximately 10× higher (Figure 5b). These particles were interpreted as bundles or aggregates of several parallel microfibrils. Some of these bundles were ramified or frayed on their ends or sometimes also on their sides (Figure 5a). The individual strings were as thick as a microfibril on their thinnest and the cavities between them could extend a length of several micrometers in the longitudinal direction of the fibres (Figure 5d). The thicknesses of the particles were interpreted to vary, since individual microfibrils inside a bundle were to be seen in some pictures, whereas in some pictures the particles were completely opaque (Figure 5c). In addition to the larger particles, few individual microfibrils were seen in the samples (Figure 5e).

Discussion

According to the WAXS results, the average crystal sizes of cellulose and the crystallinity of the sample did not change during hydrolysis. The obtained values are in agreement with earlier results for similar types of celluloses; according to Andersson et al., the degree of crystallinity in Avicel is below

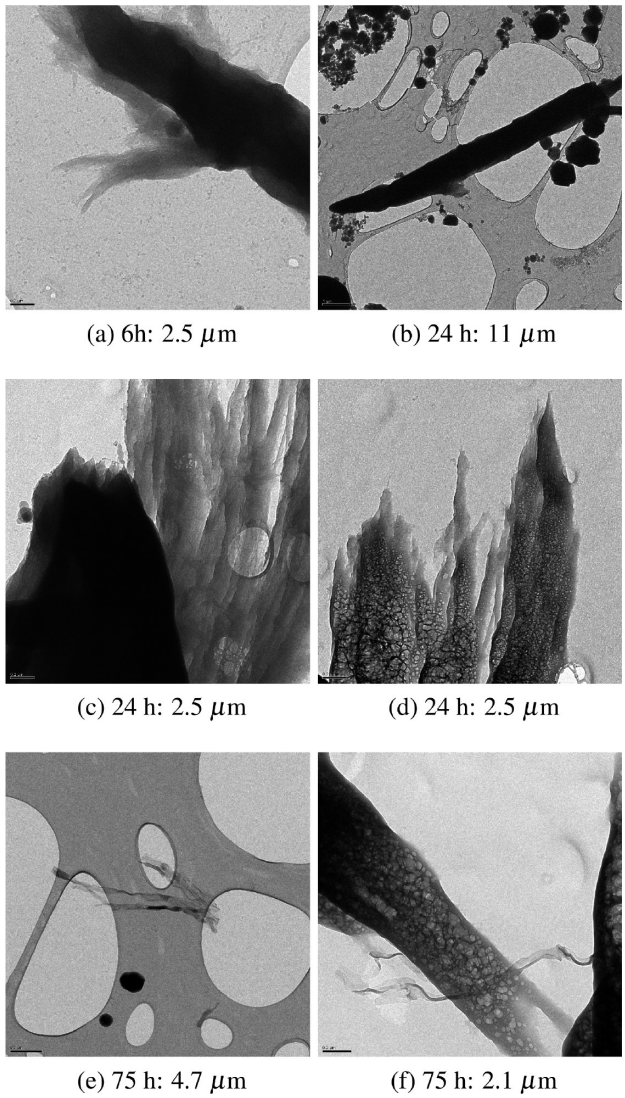

Figure 5. Collection of TEM pictures of enzymatically hydrolyzed MCC after various hydrolysis times. The length below each image indicates the length of one side of the image. The dark round-shaped objects are ice contamination and the big light circles holes in the carbon film, with which the grid was covered. The microfibril bundles are seen as partly ramified or smooth-surfaced and elongated particles. The bubbles inside of some of them are due to beam damage. Possible individual microfibrils can be seen in (e) and (f).

60%.[24] Previous studies have also shown that the crystallinity of MCC remains unchanged during hydrolysis,[4,9] which can be interpreted so that, independent of the hydrolysis time, most of each sample consists of intact cellulose fibrils. Based on this, many studies have proposed that the hydrolysis solubilizes the outermost fibrils of the aggregates one by one,[4,6] which seems a plausible interpretation also in this work. In addition, a small change in the crystallinity, as reported for instance by Wang et al. for cotton fibers during enzymatic hydrolysis,[7] could have stayed inside the error margins of this study. Concerning the crystal sizes, their behavior during hydrolysis seems to be strongly affected by the origin of the cellulosic substrate.[4,7,8] According to Gama and Mota, the crystal width of Avicel remained unchanged, whereas it decreased for the less crystalline Sigmacell during enzymatic hydrolysis.[4]

The power law behavior of the SAXS intensities was investigated on smaller q-values (Table 2). Based on the power laws, structures between 10−20 nm in wet samples and between 10−30 nm in dry samples could be described by fractal dimensions. The surface fractal dimensions of the dry samples corresponded to fairly smooth surfaces,[25] meaning that the particles were dense inside. The mass fractal dimensions of the wet samples corresponded to a more open structure formed by loose aggregates.[26] This mass fractal dimension diminished during the hydrolysis, which could mean an opening of the structures caused for instance by the enlargening of pores between the individual microfibrils or a ramification of the microfibril bundles, leading to structures like the ones observed in the TEM pictures (e.g., Figure 5d).

At this point, it must be noted that the theory concerning the interaction between water and MCC in submicrometer scale is not known exactly. A question arises, whether water can penetrate into the amorphous parts of the cellulose fibrils or not. This is an important question for the SAXS analysis, because only differences in electron density are seen by this method. If water can penetrate into the amorphous parts, the two phases visible for SAXS would be pieces of crystalline cellulose and a water matrix surrounding them. This was the assumption used in this study and its usage has been justified elsewhere.[20] The dry samples, on the other hand, would be seen as solid cellulose in air, having both the amorphous and the crystalline parts included in the same phase.

As already stated in Results, the SAXS results presented for the wet samples in Table 3 may contain some experimental error. The major source of this error was the imperfect determination of the volume fractions of water and cellulose. In the preparation of these samples, it was not guaranteed that the water would be equally dispersed in the whole sample and the total volume of the sample was not precisely the same for all samples. Thus, the actual proportion of water in the beam was hard to determine afterward and the values shown in Table 3 for the wet samples are not comparable between different hydrolysis times. For the dry samples, the determination of volume fractions was easier and the results for them are more reliable.

A minor source of error in the results of Table 3 might be the use of the density of crystalline cellulose as the density of the solid phase in all samples. A smaller density value of 1.4 g/cm^3 (the "true density" of MCC according to Sun[27]) in the analysis was observed to increase the specific surfaces of the dry samples by 50% and the same of the wet samples by 190%. Also, the average chord lengths of whole samples would have been 20 and 60% smaller for dry and wet samples, respectively. Especially the possible errors for the wet samples seem quite large, but, on the other hand, if the two phases in the wet samples are supposed to be water and crystalline cellulose, the use of the density of crystalline cellulose is justified. Also, the real density of the solid phase in the dry samples most likely settles somewhere between these extremes. In any case, the choice of the density value should have the same effect on the values from all samples, regardless of hydrolysis time.

Despite the possible inaccuracy in the actual values, the orders of magnitude of the specific surfaces and average chord lengths shown in Table 3 are representative. Similar results for dry and wet cellulose materials have been published earlier[20,28−30] and it is known that the pore structure of wet cellulose changes during drying and rewetting.[20] Wet cellulose contains a large proportion of narrow pores between individual microfibrils or small bundles of them. These pores occupy a large proportion of the total volume and yield a high specific surface. In dry cellulose, the pores are fewer and larger in their cross sections.[28−31] This explains the fact that the average chord lengths, that is, the average distances between interfaces of the phases, were 1−2 orders of magnitude larger in the dry samples

than in the wet samples. The specific surfaces were also 2 orders of magnitude smaller in the dry samples, because larger pores have substantially less surface area per volume than smaller pores.

No definite conclusions on the effects of hydrolysis on the structure of MCC can be drawn based on the results presented in Table 3. Especially the values for the wet samples behaved inconsistently as a function of hydrolysis time, which is most probably caused by the inaccuracy of the volume fractions. In spite of all, it might be possible, that the change in the values of the dry samples would correspond to a small change in the morphology. The specific surface seemed to increase slightly during hydrolysis, as the average chord length for the solid phase increased and the average chord length for the air phase decreased. Gupta and Lee as well as Wang et al. have both reported previously an increase in the specific surface of cellulose as a function of hydrolysis time,[5,7] but taking into account the inaccuracy of the results of this study, it is impossible to make further conclusions about any eventual changes.

Thus, in the SAXS measurements the only quantity which was seen to change undisputedly during hydrolysis was the fractal dimension of the wet samples. The reason why this change was seen only in the wet samples could be due to the different pore structures of wet and dry cellulose. So it might be possible that the changes during hydrolysis could be hidden inside the solid phase when the cellulose is dried and come visible again when the substance is rewetted. This phenomenon could be studied in the future by carrying out the measurements in real time or without drying. In addition, the Porod fit on larger q-values might have revealed more information on the structural changes of MCC during the hydrolysis, though the samples were not measured on that interval in this work.

In a recent study, Kent et al. studied the structure of Avicel FD100 hydrolyzed with cellulases from the *Trichoderma viride* enzyme system, accompanied by β-glucosidase from almond in some of the experiments.[9] Their main method was small-angle neutron scattering (SANS), but the samples were also characterized with scanning electron microscopy (SEM) and X-ray diffraction. The fundamental difference compared to this work was that the enzymes reacted either in a static state, that is, without any stirring or shaking, or in a dynamic state under constant agitation and motion through the sample chamber, whereas in this work the bottles were only shaken with a low rate. Despite a different enzyme origin and hydrolysis methods, their results were at least partly congruent with our results. In the SANS curves, they saw power laws on slightly different q-ranges, even though their fractal dimensions were higher and increased during the dynamic hydrolysis. They interpreted the fractal dimensions to describe the water distribution rather than the solid material, which then indicated a more compact and dense distribution of water inside the fibers. Their curves also showed a "roll-off" at $q = 0.08$ 1/Å, which disappeared in the beginning of the hydrolysis. In our results, a "roll-off" was seen at $q = 0.10$ 1/Å and it did not change during the hydrolysis. Similar to our results, their SEM images showed no change in the scale of hundreds of nanometers and according to their X-ray diffraction experiments the crystallinity index was preserved.

The results of this study support a common view of enzymatic hydrolysis of cellulosic materials.[6,7,10] According to our results, it seems that cellulase enzymes cannot penetrate into the nanopores of all MCC particles or at least cannot act synergistically in them. In contrast, the enzymes may proceed layer by layer on the outer surface of the cellulose bundles or possibly on the surfaces of larger pores inside them. Despite this, some of the bundles are already open enough toward the enzymes to enter or they may transform into such forms due to hydrolysis on their outer surface or on the surface of larger pores. This would result in an increased accessible surface for the enzymes and, hence, lead to a fast degradation of the whole bundle. This proportion of the substrate could even yield most of the total amount of glucose produced by the hydrolysis. In a similar way, Kent et al.[9] concluded that under agitation the cellulose, amorphous and crystalline on equal extents was digested around the larger pores throughout the particles. The smaller pores would not be large enough for the enzymes to penetrate. These ideas are also supported by the TEM pictures of this study, which besides giving a picture of the morphology of the micrometer-sized MCC particles, proved that there were still almost intact particles even in the last sample, where 68% of the original cellulose was degraded into glucose. The actual change between the samples was to be seen on a larger scale, for which the microtomography images provided an undisputable evidence.

Conclusions

Overcoming the bottlenecks in efficient biorefining is of a great importance to utilize the cellulosic biomass completely as a renewable energy source. Possibly the most critical step in the process is the degradation of cellulose into fermentable sugars, which requires efficient enzymatic hydrolysis. It has been shown previously that the structure and morphology of the substrate play a crucial role in the process. Therefore, the knowledge of this structure and the effect of hydrolysis on it are valuable information when searching for ways to improve the efficiency of the entire process.

In this work, the modification of the submicrometer structure of microcrystalline cellulose during the enzymatic hydrolysis was studied using X-ray scattering methods, X-ray microtomography, and transmission electron microscopy. Most of the results support the perception that the cellulase enzymes are not generally able to penetrate into the nanosized pores of cellulose. Instead, they degrade the bundles of microfibrils from the outer surface or from the surface of larger pores, proceeding layer by layer. The more easily accessible bundles are degraded faster, whereas the less easily accessible bundles can remain almost intact.

This interpretation was supported by the unchanged degree of crystallinity and crystal sizes in the WAXS results as well as the unaltered average dimensions in scale of 1−100 nm in the SAXS results. Besides the decrease of the microscale particle size seen in the tomography images, the only measure that was seen to change during the hydrolysis was the fractal dimension of the SAXS curves for wet samples in scale of 10−20 nm. This was interpreted to rise from a change in the pore structure corresponding to this length scale or a ramification of the bundles of microfibrils, which was also observed for some particles in the TEM pictures.

The results of this study may offer explanations for the gradual slowing down of enzymatic hydrolysis. Some of the substrate particles are impossible for the enzymes to penetrate into, at least without agitation. The questions apparently need more investigation, but each step is important on the way to the full usage of renewable energy sources.

Acknowledgment. The authors thank Antti Nykänen for consultation in electron microscopy. Pentti Jääskeläinen thanks Centre of Excellence in Computational Complex Systems

Research for partial support. The TEM images were taken at the Nanomicroscopy Center of Aalto University School of Science and Technology in Espoo, Finland. The work was supported by the Academy of Finland (1127759), Helsinki University funds, and Fortum Foundation.

Supporting Information Available. All equations referred to in the Experimental Section and a more detailed description on the analysis of scattering data. This material is available free of charge via the Internet at http://pubs.acs.org.

References and Notes

(1) Himmel, M. E.; Ding, S.-Y.; Johnson, D. K.; Adney, W. S.; Nimlos, M. R.; Brady, J. W.; Foust, T. D. *Science* **2007**, *315*, 804–807.
(2) Jørgensen, H.; Kristensen, J. B.; Felby, C. *Biofuels, Bioprod. Biorefin.* **2007**, *1*, 119–134.
(3) Teeri, T. T. *Tibtech* **1997**, *15*, 160–167.
(4) Gama, F. M.; Mota, M. *Biocatal. Biotransform.* **1997**, *15*, 221–236.
(5) Gupta, R.; Lee, Y. Y. *Biotechnol. Bioeng.* **2009**, *102*, 1570–1581.
(6) Zhou, W.; Schüttler, H.-B.; Hao, Z.; Xu, Y. *Biotechnol. Bioeng.* **2009**, *104*, 261–274.
(7) Wang, L.; Zhang, Y.; Gao, P.; Shi, D.; Liu, H.; Gao, H. *Biotechnol. Bioeng.* **2006**, *93*, 443–456.
(8) Cao, Y.; Tan, H. *Enzyme Microb. Technol.* **2005**, *36*, 314–317.
(9) Kent, M. S.; Cheng, G.; Murton, J. K.; Carles, E. L.; Dibble, D. C.; Zendejas, F.; Rodriquez, M. A.; Tran, H.; Holmes, B.; Simmons, B. A.; Knierim, B.; Auer, M.; Banuelos, J. L.; Urquidi, J.; Hjelm, R. P. *Biomacromolecules* **2010**, *11*, 357–368.
(10) Gama, F. M.; Teixeira, J. A.; Mota, M. *Biotechnol. Bioeng.* **1994**, *43*, 381–387.
(11) Jungnikl, K.; Paris, O.; Fratzl, P.; Burgert, I. *Cellulose* **2008**, *15*, 407–418.
(12) Vainio, U.; Maximova, N.; Hortling, B.; Laine, J.; Stenius, P.; Simola, L. K.; Gravitis, J.; Serimaa, R. *Langmuir* **2004**, *20*, 9736–9744.
(13) Miller, G. L. *Anal. Chem.* **1959**, *31*, 426–428.
(14) Stock, S. R. *Int. Mater. Rev.* **1999**, *44*, 141–164.
(15) Andersson, S.; Serimaa, R.; Paakkari, T.; Saranpää, P.; Pesonen, E. *J. Wood Sci.* **2003**, *49*, 531–537.
(16) Nishiyama, Y.; Langan, P.; Chanzy, H. *J. Am. Chem. Soc.* **2002**, *124*, 9074–9082.
(17) Porod, G. General theory. In *Small Angle X-ray Scattering*; Glatter, O., Kratky, O., Eds.; Academic Press: London, 1982.
(18) Spalla, O.; Lyonnard, S.; Testard, F. *J. Appl. Crystallogr.* **2003**, *36*, 338–347.
(19) Ishii, D.; Kanazawa, Y.; Tatsumi, D.; Matsumoto, T. *J. Appl. Polym. Sci.* **2007**, *103*, 3976–3984.
(20) Vickers, M. E.; Briggs, N. P.; Ibbett, R. N.; Payne, J. J.; Smith, S. B. *Polymer* **2001**, *42*, 8241–8248.
(21) Schmidt, P. W. *J. Appl. Crystallogr.* **1991**, *24*, 414–435.
(22) NIST, 4.8; http://physics.nist.gov/, accessed 2009.
(23) Svergun, D. I.; Koch, M. H. J. *Rep. Prog. Phys.* **2003**, *66*, 1735–1782.
(24) Andersson, S.; Wikberg, H.; Pesonen, E.; Maunu, S. L.; Serimaa, R. *Trees* **2004**, *18*, 346–353.
(25) Ishii, D.; Tatsumi, D.; Matsumoto, T. *Biomacromolecules* **2003**, *4*, 1238–1243.
(26) Lenz, J.; Schurz, J. *Holzforschung* **1990**, *44*, 227–228.
(27) Sun, C. C. *Int. J. Pharm.* **2008**, *346*, 93–101.
(28) Crawshaw, J.; Bras, W.; Mant, G. R.; Cameron, R. E. *J. Appl. Polym. Sci.* **2002**, *83*, 1209–1218.
(29) Papirer, E.; Brendle, E.; Balard, H.; Vergelati, C. *J. Adhes. Sci. Technol.* **2000**, *14*, 321–337.
(30) Yu, X.; Atalla, R. H. *Powder Technol.* **1998**, *98*, 135–138.
(31) Luukkonen, P.; Maloney, T.; Rantanen, J.; Paulapuro, H.; Yliruusi, J. *Pharm. Res.* **2001**, *318*, 1562–1569.

BM1001119